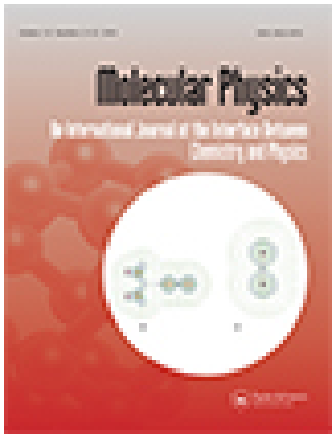

Molecular Physics: An International Journal at the Interface Between Chemistry and Physics
Publication details, including instructions for authors and subscription information:
http://www.tandfonline.com/loi/tmph20

A corresponding-states framework for the description of the Mie family of intermolecular potentials

N.S. Ramrattan[a], C. Avendaño[a], E.A. Müller[a] & A. Galindo[a]
[a] Department of Chemical Engineering, Centre for Process Systems Engineering, Imperial College London SW7 2AZ, London, United Kingdom
Published online: 01 Apr 2015.

Molecular Physics, 2015
http://dx.doi.org/10.1080/00268976.2015.1025112

SPECIAL ISSUE IN HONOUR OF TOMAS BOUBLIK, IVO NEZBEDA, THE CZECH SCHOOL OF STATISTICAL MECHANICS AND THE LIBLICE CONFERENCE

A corresponding-states framework for the description of the Mie family of intermolecular potentials

N.S. Ramrattan, C. Avendaño[†], E.A. Müller and A. Galindo[*]

Department of Chemical Engineering, Centre for Process Systems Engineering, Imperial College London SW7 2AZ, London, United Kingdom

(*Received 13 November 2014; accepted 25 February 2015*)

The Mie (λ_r, λ_a) intermolecular pair potential has been suggested as an alternative to the traditional Lennard–Jones (12–6) potential for modelling real systems both via simulation and theory as its implementation leads to an accuracy and flexibility in the determination of thermophysical properties that cannot be obtained when potentials of fixed range are considered. An additional advantage of using variable-range potentials is noted in the development of coarse-grained models where, as the superatoms become larger, the effective potentials are seen to become softer. However, the larger number of parameters that characterise the Mie potential (λ_r, λ_a, σ, ε) can hinder a rational study of the particular effects that each individual parameter have on the observed thermodynamic properties and phase equilibria, and higher degeneracy of models is observed. Here a three-parameter corresponding states model is presented in which a cohesive third parameter α is proposed following a perturbation expansion and assuming a mean-field limit. It is shown that in this approximation the free energy of any two Mie systems sharing the same value of α will be the same. The parameter α is an explicit function of the repulsive and attractive exponents and consequently dictates the form of the intermolecular pair potential. Molecular dynamics simulations of a variety of Mie systems over a range of values of α are carried out and the solid–liquid, liquid–vapour and vapour–solid phase boundaries for the systems considered are presented. Using the simulation data, we confirm that systems of the same α exhibit conformal phase behaviour for the fluid-phase properties as well as for the solid–fluid boundary, although larger differences are noted in the solid region; these can be related to the approximations in the definition of the parameter. Furthermore, it is found that the temperature range over which the vapour–liquid envelope of a given Mie system is stable follows a linear dependency with α when expressed as the ratio of the critical–point temperature to the triple–point temperature. The limit where potentials of the Mie family will not present a stable fluid envelope is predicted in terms of the parameter α and the result is found to be in excellent agreement with previous studies. This unique relation between the fluid range and the cohesive parameter α is shown to be useful to limit the pairs of Mie exponents that can be used in coarse-grained potentials to treat real systems in order to obtain temperature ranges of stability for the fluid envelope consistent with experiment.

Keywords: corresponding states; conformality; Mie potential; global phase behaviour

1. Introduction

The pairwise approximation that is adopted from the outset in many statistical mechanics-based approaches (be it theory or simulation) results in the need for proposing an effective intermolecular pair potential to describe the interactions between model particles. In the simplest models, spherically symmetric potentials are used and it is acknowledged that a balance of repulsive and attractive forces is needed to reproduce the thermodynamic properties (specifically the phase behaviour) of most real systems. This idea is very nicely described by Lennard– Jones [1] in his seminal 'Cohesion' paper where he writes: 'There are in nature, as in politics, two opposing forces. One of these aims at a peaceful consolidation and the other at a more active and probably more spectacular disruptive process.' Well-known examples of spherically symmetrical potentials that incorporate intermolecular repulsion and attraction are the square-well (SW), Sutherland [2,3], Yukawa [4], Morse [5], Buckingham [6] and, of course, the Lennard–Jones (LJ) [7] models.

The latter is the most widely used for describing the interaction of simple non–polar molecules. It can be expressed as

$$u^{\mathrm{LJ}}(r) = 4\varepsilon\left[\left(\frac{\sigma}{r}\right)^{12} - \left(\frac{\sigma}{r}\right)^{6}\right], \tag{1}$$

where r is the centre–centre distance, σ is the distance at which the potential is zero, hence providing a lengthscale, and ε is the potential energy well minimum. Addressing the need for repulsive and attractive interactions, a repulsive term proportional to r^{-12} and an attractive one proportional to r^{-6} are built in. While there are theoretical arguments

[*] Corresponding author. Email: a.galindo@imperial.ac.uk
[†] Current address: School of Chemical Engineering and Analytical Science, The University of Manchester, Manchester, M13 9PL, United Kingdom

to support the value of 6 for the attractive exponent [8,9], there is no fundamental basis for the choice in the repulsive form, and there has been some debate regarding 12 as being an appropriate choice for describing the properties of real substances. Lennard– Jones himself suggested the use of a repulsive exponent of 13 1/3 to model argon [7]. It makes sense then to recognise the somewhat empirical nature of the LJ potential and to use both exponents as adjustable parameters. Such a generalisation had already been hinted from different arguments by Mie in 1903 [10]. In modern form, the expression of the Mie potential can be given as

$$u^{\text{Mie}}(r) = \mathcal{C}\varepsilon\left[\left(\frac{\sigma}{r}\right)^{\lambda_r} - \left(\frac{\sigma}{r}\right)^{\lambda_a}\right], \tag{2}$$

where

$$\mathcal{C} = \left(\frac{\lambda_r}{\lambda_r - \lambda_a}\right)\left(\frac{\lambda_r}{\lambda_a}\right)^{\lambda_a/(\lambda_r-\lambda_a)}, \tag{3}$$

and λ_r and λ_a are the repulsive and attractive exponents, respectively. The Mie intermolecular pair potential is therefore characterised uniquely by four parameters: the energy well-depth ε, the characteristic length σ and the exponents, which dictate the overall potential form. The additional degrees of freedom provided by treating λ_r and λ_a as variables afford the Mie potential a better performance in describing the phase behaviour of complex systems as compared to the traditional LJ model. An early recognition of this was the implementation of the Mie potential for the development of coarse-grained force fields for use in computer simulation calculations by Klein and co-workers [11–13]. More recently, Potoff and Bernard-Brunel [14] have developed transferable united-atom force fields based on (λ_r,6) Mie potentials that can be used to compute the equilibrium thermodynamic properties of the *n*-alkane and *n*-perfluoroalkane homologous series. They observe that by altering the repulsive range of the potential an accurate description of the vapour pressures of these systems can be provided while maintaining accuracy in the calculated values of the saturated liquid densities; the use of a fixed-range LJ potential does not allow a similarly accurate description of both equilibrium properties. A more detailed review of the history of these classical empirical potentials has been given in the introduction of Lafitte *et al*. [15] and in [16].

The parameterisation of force fields for the description of real systems via computer simulation can be a time-consuming iterative process and often only a limited amount of experimental data are used in model development and validation. This is one of the reasons that has made the LJ potential so extensively used in force-field development; it only requires two parameters to be adjusted, while the extent to which it might not provide a consistently accurate representation of a range of thermodynamic properties has only been highlighted recently. In a case study based on CO_2, the advantages of using coarse–grained force fields based on Mie potentials has been highlighted [17]. In the latter work, a single spherical Mie site is used to reproduce a broad range of thermodynamic properties such as isotherms, vapour pressure, vapour–liquid equilibrium as well as surface tension, enthalpy of vapourisation, coefficient of thermal expansion, isothermal compressibility, speed of sound and the Joule-Thomson coefficient over the entire fluid range using molecular simulations. The parameterisation of the potential in [17] was carried out taking advantage of an accurate equation of state (EOS), the statistical associating fluid theory for potentials of variable range (SAFT-VR) that effectively reproduces the simulation data based on the Mie potential [15,18]. In implementations of molecular models via analytical equations of state, the evaluation of thermodynamic properties is computationally very cheap, so that the parameters most suited for the representation of the experimental properties of a given substance or mixture can be obtained using fast numerical methods to minimise defined objective functions that measure the deviation between the calculated and experimental data. Thus, usually a large amount of experimental data over wide thermodynamic conditions can be used to develop and validate the potential model parameters associated with equations of state, though accuracy of the equation of state can be an issue. The increasing interest in the Mie potential has prompted the development of molecular-based equations of state that implement this potential [15,18–20]. The SAFT-VR Mie equation of state [15] yields an evaluation of the fluid thermodynamic properties that is effectively as accurate as the simulated data as shown in [15,17]. Maginn and co-workers have used the same single-site force field of carbon dioxide to carry out extensive calculations of the thermodynamic and transport properties of carbon dioxide over broad thermodynamic conditions as well as in mixtures with methane, and to compare with other force fields [21–23]. Overall, the model is seen to perform very well, especially considering its simplicity. The same SAFT-VR Mie-based coarse-graining methodology has been used to treat *n*-alkanes, a refrigerant (HFO-1234yf), perfluoromethane (CF_4) and sulfur hexafluoride (SF_6) [24], and benzene and *n*-decylbenzene in another work [25]. A review of this top-down parameterisation method is given in [26].

The works of Klein and co-workers [11–13], Potoff and Bernard-Brunel [14] and those from our group [17,24,25] showcase the advantages of using a generalised Lennard–Jonesium (Mie) potential of varying exponents λ_r and λ_a in the development of force fields for the description of fluid properties of real systems. As the exponents change, however, it is important to consider also the impact that the choice of potential can have on the global stability of the vapour–liquid equilibrium region. In 1992, Girifalco [27] proposed an effective pair potential to describe the interactions of between furellene (C_{60}) molecules at high temperature that was based on a Mie potential of steeper repulsion

and shorter range than the traditional LJ form. A year later, Hagen *et al*. [28] mapped out using computer simulation calculations the phase diagram corresponding to the Girifalco model. They performed Gibbs-ensemble Monte Carlo [29] simulations for the fluid phases and free energy calculations coupled with the Gibbs–Duhem integration technique [30] for the solid-fluid transitions observing only the solid and vapour phases to be stable (i.e., the liquid–vapour envelope of the Girifalco potential is metastable). Since then, further works have recognised that the existence of a stable vapour–liquid coexistence region is directly linked to the range of attraction and repulsion of the pair potential [31–34]. Hagen and Frenkel [31] performed computer simulation calculations of the hard-core Yukawa family of potentials and showed that a faster decaying attractive tail in the potential leads to a widening of the solid–fluid region and to a metastable fluid envelope. In terms of the Mie family, Hasegawa [32] and Hasegawa and Ohno [33] carried out variation perturbation calculations as well as density functional theory calculations of freezing, respectively, to study the family of ($\lambda_r = 2\lambda_a$, λ_a) systems. The two approaches produced similar results and confirmed the relation of the stability of the vapour–liquid equilibrium region and the degree of attraction between particles. Lekkerkerker and co-workers have also shown that the vapour–liquid critical temperature is lowered by increasing the repulsive interaction of the potential [34] and have proposed a predictive method of finding the critical point of any Mie potential by the use of the second virial coefficient, which they show to be insensitive to the value of the repulsive exponent at the critical temperature [35]. Furthermore, Ahmed and Sadus [36] have carried out MD simulations to study the effect of the repulsive exponent on the solid–fluid coexistence and the triple–point properties (estimated by extrapolation) for the (12,6), (11,6), (10,6), (9,6), (8,6) and (7,6) Mie model systems. These values were then used to determine the triple–point data for the infinitely repulsive case ($\lambda_r \rightarrow \infty$). One of the most recent studies on the stability of the liquid phase with variation of inter–particle repulsion is an experimental study by Larsen and Zukoski [37], who, through the analysis of colloidal interactions, find that the range of attraction also plays a critical role in determining whether a system will possess a stable liquid phase, hence confirming previous simulation studies. They propose the use of a variable which is a ratio of the energies of the liquid and solid phases, which can be used to determine the stability of the liquid phase. Unfortunately, the Mie potential is not explicitly studied in their work, but the analysis provides sound experimental evidence to elucidate the mechanisms through which a system will exhibit a metastable liquid state, liquid-like or solid-like behaviour.

Perhaps motivated by the larger number of parameters that characterise the Mie potential as compared to the traditional LJ, it has also been of interest for sometime to rationalise the behaviour of the Mie family of systems in terms of a corresponding-states (CS) approach. Okumura and Yonezawa [38] carried out molecular dynamics (MD) simulations in the isobaric– isothermal ensemble combined with calculations using the test-particle methods to calculate the fluid–phase boundaries of the (λ_r, 6) family over a range λ_r= 7–32 and show that the vapour–liquid envelopes of the fluids tested collapse to a master curve when reduced with respect to critical properties; although they also note a linear dependence of the critical properties on the range of attraction of the potential model. Later, Orea *et al*. [39] studied the vapour–liquid equilibrium and interfacial properties of several other combinations of repulsive and attractive exponents using canonical Monte Carlo simulations. They present the saturated vapour–liquid curve, surface tension plots and pressure–density plots in terms of calculated/simulated critical properties of the respective fluids using $T_r = T/T_c$ for the reduced temperature, $P_r = P/P_c$ for the reduced pressure, $\rho_r = \rho/\rho_c$ for the reduced density, and $\gamma_r = \frac{\gamma}{\rho_c^{2/3} T_c}$ for the reduced surface tension. They note that the resulting curves roughly align to a single master curve for each of the properties considered, suggesting that irrespective of the choice of potential exponents (λ_r and λ_a), the family of Mie fluids can be characterised by σ and ε alone (as would correspond to a two-parameter CS model). However, this result is somewhat surprising, as it is known, for example, that the SW family of potentials (for which the attractive range is also variable) is non-conformal [40].

In contrast to the works of Orea *et al*. [39] and Okumura and Yonezawa [38], there have been other studies which suggest that the Mie family of systems may not follow a simple two-parameter CS model. Bulavin and Kulinskii [41] and Kulinskii [42] follow a theoretical analysis (which is confirmed by the simulation data of Vliegenthart *et al*. [34]) to propose the use of a third parameter z dependent on the critical temperature of a given Mie fluid for the scaling of properties of the Mie family of potentials. Galliéro *et al*. [20,43], have also found a dependence of the reduced pressure for (λ_r,6) fluids ranging from λ_r=10–20 with the repulsive exponent. They show how reduced pressure, P_r, of a given Mie fluid differs from the reduced pressure of the LJ model (used as a reference for comparison); this difference is noted to increase with the increasing density. In a later study of the interfacial properties of the Mie family of fluids, it is however shown that a unique scaling law can be proposed that leads to an accurate estimation of the interfacial tension of these systems [44].

These apparently contradicting CS studies and the recent interest in the use of Mie potentials to describe real systems prompt our current work. We examine the global (solid–liquid–vapour) phase diagram of these systems and propose a criterion for the characterisation of potentials based on satisfying the experimental fluid range (defined as the range of temperatures over which the gas–liquid envelope is stable, limited by the solid–liquid–vapour triple point temperature and the vapour–liquid critical temperature). We

show that through the use of the integrated mean–field energy, the Mie family of potentials can be formulated, to an approximation, as a three-parameter CS model. The model presented is validated against MD simulations, which are carried out to determine the global (solid–liquid–vapour) phase behaviour of several Mie systems. The third parameter presented relates the repulsive and attractive exponents of the potential and can be related to the experimental fluid range of a given substance. The methodology through which we define the conformality of Mie systems and the derivation of the third parameter is presented in Section 2. In Section 3, the computer simulation details are summarised and results are provided in Section 4.

2. The corresponding-states principle and conformality through the free energy

The CS principle is based on the underlying assumption that there is a common functional form that can be used to describe the thermodynamic properties of any fluid, regardless of the substance. It was first suggested theoretically by van der Waals [45] who derived it from his well-known EOS in the following form:

$$P_r = \frac{8T_r}{(3V_r - 1)} - \left(\frac{3}{V_r^2}\right), \tag{4}$$

where a reduced temperature $T_r = T/T_c$, volume $V_r = V/V_c$ and pressure $P_r = P/P_c$ are defined in terms of their respective critical properties T_c, P_c and V_c. A key contribution of the CS idea is that the experimentally known configurational properties of a few substances can be used to predict the values of the same properties for fluids which have not been studied experimentally. It was by following these suggestions that Kamerlingh-Onnes [46] first liquified helium. The pioneering experimental studies of Guggenheim [47] and Su [48] provided evidence that the properties of simple fluids can be shown to follow a unique master curve when reduced with respect to their critical properties. The work of Guggenheim, in particular, is noteworthy as it was the first experimental work to analyse thermophysical properties such as the vapour–liquid curve, second virial coefficient, Boyle point, vapour pressure, entropy of vapour, coefficients of thermal expansion, triple–point properties and surface tension of liquid argon, krypton, xenon and neon systematically. The thermodynamic properties studied for these substances were found to follow the CS principle. Nitrogen, oxygen, carbon monoxide and methane were also analysed [47] and were also found to conform to a unique vapour–liquid curve. Guggenheim also noted that although the fluid phases follow the CS principle, this was not true for the solid phase.

It is important to note that the CS principle is not a universal law but rather an experimental observation valid within a range of conditions and for substances of similar morphology and chemical nature. This is noted by contrasting the excellent agreement shown by the noble gases when tested against the list of properties investigated by Guggenheim, with that of more complex fluids and for a number of other properties, the conformal behaviour is not followed as precisely. For example, even simple almost-spherical compounds such as CH_4 do not follow quantitatively the reduced properties of the noble gases. Although the CS principle was originally an empirical observation, a statistical mechanics basis for the idea was provided by Pitzer [49] in 1939. His work clarified the approximations made and confirmed that the CS principle should be extendable to more complex systems [50]. The derivation of the CS principle from statistical mechanics along with the assumptions which are commonly applied can be found in a review by Leland and Chapplear [51] and in [50] alongside the original paper [49]. Although we do not study mixtures in this work, we mention briefly at this point the interesting works of Longuet-Higgins [52] in the development of the theory of conformal solutions, which constitutes an extension of the principle of CS and the relation presented by Pitzer [49], and the work of Brown [53] who specifically considered mixtures of spherical particles interacting via LJ potentials of general form (Mie potentials).

The key assumption of Pitzer is the existence of a universal function of a pairwise potential for two spherically symmetric particles which can be non-dimensionalised in terms of the model parameters characteristic for a given substance. In two-parameter CS models, the underlying assumption is that for most simple spherical fluids only repulsive and dispersive forces are important; hence two scales, one of energy and the other of distance, are deemed sufficient to map the fluid behaviour. The molecular requirements that must be satisfied for a system to obey the CS principle in its simplest form are outlined in the original paper [49]. The two independent scaling parameters (ε and σ) may then be employed to non-dimensionalise (reduce) macroscopic properties. For example, dimensionless variables $T^* = k_B T/\varepsilon$, $P^* = P\sigma^3/\varepsilon$ and $\rho^* = \rho\sigma^3$ are proposed relating the intermolecular potential parameters ε and σ to experimental properties. Using these variables the EOS can be expressed in the form

$$P^* = f(T^*, \rho^*). \tag{5}$$

A direct application of this concept is the determination of the molecular model parameters using the EOS to compare experimental and calculated fluid properties for different sets of parameters [50]. Note that the EOS does not need to have an analytical form; computer simulation data can be used equally. Moreover, note that if two (or more) systems can be described by the same expression of the free energy at given reduced temperature and density, they will also have identical macroscopic thermodynamic properties and in essence they will be conformal [49]. This concept has

been previously applied to a range of fluids such as SW, Yukawa, Sutherland and Mie systems [54].

We hence start with a plausible set of descriptors for the free energy of simple fluids, namely the Barker–Henderson (BH) [55,56] perturbation theory, carrying out a high-temperature expansion of the Helmholtz free energy to first order for the Mie pair potential. In the perturbation theory of BH, the full pair potential is treated as the sum of a reference system $u_0(r)$ and a perturbation term $u_1(r)$, i.e.,

$$u^{\text{Mie}}(r) = u_0(r) + u_1(r). \tag{6}$$

In the case of a Mie potential as written in Equation (2),

$$u_0(r) = \begin{cases} u^{\text{Mie}}(r) & r \le \sigma \\ 0 & r > \sigma, \end{cases} \tag{7}$$

and

$$u_1(r) = \begin{cases} 0 & r \le \sigma \\ u^{\text{Mie}}(r) & r > \sigma. \end{cases} \tag{8}$$

Barker and Henderson [55,56] showed that it is then possible to write the Helmholtz free energy A of the full system as a high-temperature expansion of free energy terms. Each of the residual terms is dependent on the corresponding thermodynamic variables and pair potential parameters. Thus,

$$\begin{aligned} a(T, \rho; \sigma, \varepsilon, \lambda_r, \lambda_a) = a^{\text{id}}(T, \rho) + a_0(T, \rho; \sigma, \lambda_r, \lambda_a) \\ + \beta a_1(T, \rho; \sigma, \varepsilon, \lambda_r, \lambda_a) \\ + \mathcal{O}(\beta^2) + \cdots, \end{aligned} \tag{9}$$

where $a = A/(Nk_{\text{B}}T)$, a^{id} corresponds to the ideal free energy, a_0 to the free energy of the reference system and a_1 to the first-order perturbation term, with β representing the inverse of temperature $\beta = 1/(k_{\text{B}}T)$, k_{B} is the Boltzmann constant, N the number of particles and $\rho = N/V$ the number density. The second-order and higher-order terms of the expansion are neglected here. We follow from this expression to show, to a level of approximation, that the family of Mie potentials can be reduced to a three-parameter CS model.

We assume that although free energy of the reference term is strictly a function of σ, λ_r and λ_a, the potential is steep enough to be treated as repulsive potential function of σ (and density) only,

$$a_0(T, \rho; \sigma, \lambda_r, \lambda_a) \approx a_0^{\text{HS}}(T, \rho; \sigma), \tag{10}$$

where a_0^{HS} refers to a purely repulsive hard-sphere system. The impact of this approximation will be apparent later. This free energy if needed, may be evaluated via an accurate equation of state such as that of Carnahan and Starling [57] for a fluid or the Hall equation for solids [58] or via computer simulation. We also note here that a very accurate evaluation of the Helmholtz free energy of a fluid mixture of hard spheres can be obtained with the equation of state first presented by Thomas Boublík [59], to whom this Special Issue is dedicated.

The first–order perturbation term is given as [55,56]

$$a_1(T, \rho; \sigma, \varepsilon, \lambda_r, \lambda_a) = 2\pi\rho \int_{\sigma}^{\infty} g_0(r) u_1(r) r^2 dr, \tag{11}$$

where $g_0(r)$ is the radial distribution function of the corresponding reference system. If a mean–field approximation is assumed, where $g_0(r) = 1$, the first–order perturbation term is then given as

$$a_1^{\text{MF}} = -2\pi\rho\varepsilon\sigma^3 \mathcal{C} \left[\left(\frac{1}{\lambda_a - 3} \right) - \left(\frac{1}{\lambda_r - 3} \right) \right], \tag{12}$$

which allows to define a new parameter

$$\alpha = \mathcal{C} \left[\left(\frac{1}{\lambda_a - 3} \right) - \left(\frac{1}{\lambda_r - 3} \right) \right] \tag{13}$$

that relates the repulsive and attractive exponents of the potential, and to write the first–order mean-field perturbation term as

$$a_1^{\text{MF}}(T, \rho; \varepsilon, \sigma, \alpha) = -2\pi\rho\varepsilon\sigma^3\alpha. \tag{14}$$

We note, of course, that a mean-field treatment of the solid phase will be less accurate than in the fluid phases.

Examining the arguments above, it can be seen that at a given temperature and density Mie systems of the same ε, σ and α will have the same free energy; hence the same properties and therefore will be conformal. The parameter α depends solely on the repulsive and attractive exponents of the pair potential and constitutes a dimensionless third parameter that determines the free energy of the Mie fluid under consideration. This derivation suggests that the Mie potential is not conformal for any given pair of exponents (λ_r, λ_a) but rather only for those that yield the same value of α. This result also suggests that the Mie family cannot be universally mapped to a unique master curve as an exclusive function of ε and σ as suggested by Orea *et al.* [39] and Okumura and Yonezawa [38]. In the following sections, we carry out MD simulations to study Mie systems of varying α to investigate this proposition.

3. Simulation details

MD simulations are performed to determine the phase boundaries of a number of systems interacting via Mie pair potentials selected in terms of the value of the parameter α presented above. The MD code DL_POLY (version 2.20) [60] is used to perform all calculations, with the

Nosé–Hoover thermostat implemented to ensure an average constant temperature throughout the timescale of each simulation. The equations of motion are integrated using the velocity Verlet algorithm using periodic boundary conditions in the three directions. The system sizes are chosen such that finite size effects are negligible and a cut–off radius of 5σ is employed. No long–range corrections are employed in any of the states considered. A longer cut-off radius (7σ) was investigated and did not result in any significant change of the calculated coexisting densities (within the error of the simulations) even for the softest (longest range) potential employed, hence validating the exclusion of long-range corrections.

The vapour–liquid phase boundary was determined carrying out canonical *NVT* simulations with $N = 2400$ particles in an orthorhombic box of relative dimensions $L_x = L_y = L$ and $L_z \geq 3L$. An initial unstable configuration inside the phase boundary is prepared at low temperature, once phase separation is achieved, simulations of increasing temperature are performed, each from the previous configuration. Each state point is run for 10^6 time steps (time steps of $\delta t = \Delta t(\varepsilon/(m\sigma^2))^{1/2} = 0.02$, where $\delta\, t$ is the time step in seconds with the first 40% of the configurations discarded to ensure equilibration. The liquid– vapour coexistence densities are obtained from the density profile taken along the z–axis of the simulation box at each temperature. The vapour pressure is obtained from the P_{zz} component of the pressure tensor, normal to the interface, obtained via the virial route. Values for the critical temperature T_c^* and density ρ_c^* are obtained by fitting to subcritical data, using the simulation results for the liquid and vapour densities and the relations [61]:

$$\rho_l^* = \rho_c^* + C_2 \left|1 - \frac{T^*}{T_c^*}\right| + \frac{1}{2} B_0 \left|1 - \frac{T^*}{T_c^*}\right|^{\beta} \tag{15}$$

and

$$\rho_v^* = \rho_c^* + C_2 \left|1 - \frac{T^*}{T_c^*}\right| - \frac{1}{2} B_0 \left|1 - \frac{T^*}{T_c^*}\right|^{\beta}, \tag{16}$$

where ρ_l^* and ρ_v^* are the liquid and vapour coexistence densities at temperature T^*. The critical density and coefficients B_0 and C_2 are constants to be determined, and $\beta = 0.325$ is the universal critical exponent obtained from renormalisation group theory. The critical pressure P_c^* is obtained by extrapolation using the Clausius–Clapeyron equation.

The solid–fluid equilibrium boundary is particularly difficult to obtain from computer simulation due to the timescales involved and the high density of the phases. Here we use a direct simulation method in which the two phases are in contact in one simulation box. We refer to our method as the 'freeze' method [62]. A number of similar direct simulation methods for the solid–fluid boundary have already been presented by other authors and have been shown to be accurate [63–65]. It is worth mentioning also the recent work of Nayhouse *et al*. [66] who have proposed a new method for the determination of solid–liquid boundaries based on cell models. In our direct approach, the solid and liquid phases are in contact in a 4×1 simulation box. The method allows for an accurate determination of solid–fluid coexistence properties by combining pure solid and fluid phases at estimated conditions close to coexistence, which reduces the time required for the solid phase to melt and for the formation of a stable interface and phase equilibrium to be established. In order to select an appropriate initial state with the correct solid structure and overall appropriate density (corresponding to a density inside the phase boundaries), preliminary simulations are carried out in the isobaric–isothermal ensemble at different temperatures along an isobar. A solid phase is prepared starting from an fcc lattice at low temperature and is slowly heated at constant pressure until melting is observed; constant stress simulations are carried out to allow for deformations of the box. A cooling isobar is also run, starting from a gas-like configuration at high temperature which is cooled along the isobar until a discontinuous change in density is observed. A hysteresis region is usually observed, and a temperature and total density inside the hysteresis region are then selected.

The last stable solid configuration of the heating branch is replicated four times along the z–direction of the simulation box. Half of this system is 'frozen' (i.e., the particles in one half of the box are at this point fixed in space). A number of molecules in the other half of the box, which are allowed to move in the usual way, are then removed [67]. The number of molecules to be deleted is calculated from the estimated total density inside the metastable region identified in the preliminary simulations locating the hysteresis region. This configuration is run in the canonical *NVT* ensemble, 10^6 time steps are usually enough to induce melting in the region of lower density where the particles have been deleted. The solid molecules are then 'unfrozen' and the complete system is run for another 5×10^6 time steps, with 20% of these discarded for equilibration. The density profile of a successful simulation presents two well-defined plateaus corresponding to the densities of the two coexisting phases. If the entire simulation either melts or freezes, an iterative process is implemented to either reduce or increase the number of molecules that are removed from the replicated cells and the procedure repeated until coexistence is obtained. The equilibrium pressure is obtained from the normal component of the pressure tensor, and to ensure the accuracy of the calculation, single-site *NVT* simulations at the coexistence densities obtained from the density profile are also carried out and the pressures are checked. Once an accurate coexistence point is obtained, the Gibbs–Duhem integration method [30] is implemented to trace the solid–fluid boundaries at other pressures, although we note that in cases in which the solid–fluid

boundaries are very steep, it is found to be more computationally efficient to heat/cool the known coexistence point with the two phases in direct contact.

The solid–vapour equilibrium boundaries are determined assuming coexistence between a solid phase and a gas, using constant stress $N\sigma T$ simulations [68] at zero pressure over a period of 10^6 time steps with the first 40% being discarded to ensure equilibration. For all simulations performed, the error in the calculation is also determined. For pure phase NPT or $N\sigma T$ simulations, the associated error in the density is obtained from the fluctuation in the size of the simulation cell. For pure phase NVT simulations, the error in the pressure is obtained from the fluctuations in the pressure tensor. For NVT phase coexistence simulations, the error in the coexisting densities is calculated as the maximum deviation from the averaged coexistence value obtained from the density profile. These are found to be of the order of 10^{-3} in all cases. The triple point is estimated from the intercept of the liquid boundaries of the vapour–liquid envelope and the solid–liquid boundary using best-fit trendlines. A larger error that 10^{-3} can be expected for these data.

4. Results

4.1. Validation of the use of α to determine conformal Mie systems

We have discussed in Section 2 how a parameter α (Equation (13)) can be proposed such that systems of the Mie family of pair potentials with the same α will exhibit the same thermodynamic properties, and hence the same phase behaviour. To validate this idea we calculate the fluid-phase coexistence properties (saturation densities and vapour pressure) of four Mie fluids which are characterised by different exponents (λ_r,λ_a) but that correspond to two values of α as calculated via Equation (13). The first system considered (Model 1) is inspired by the coarse–grained model of CO_2 presented in [24], where a single-site Mie potential of repulsive exponent $\lambda_r = 26.00$ and attractive exponent $\lambda_a = 6.66$ was shown to yield accurate single-phase and coexistence properties over a wide range of thermodynamic conditions, including thermodynamic states not used in the parametrisation of the model. This model has a value of α corresponding to $\alpha = 0.521$. A second Mie pair-potential model (Model 2) with the same value of α but different exponents ($\lambda_r = 14.65$ and $\lambda_a = 8.00$) is selected in order to compare the thermodynamic properties of the two systems. In addition, the phase behaviour of these two fluids is also compared to that of the LJ (12.00, 6.00) model which has a corresponding $\alpha = 0.889$ and a third model system (Model 3) characterised by exponents (9.16,7.00) which shares the same value of $\alpha = 0.889$ as the LJ model.

In Figure 1(a), the vapour–liquid equilibrium boundaries for the four models are presented as temperature–density phase diagrams. In Figure 1(a), the properties are scaled in terms of each of the corresponding critical temperatures and densities (T_r=T^*/T_c^* and $\rho_r = \rho^*/\rho_c^*$) (cf. Table 1 for the calculated critical states). The fluid-phase boundaries of the four systems in this representation overlap on one unique curve, in accordance with the findings of Orea *et al*. [39] and Okumura and Yonezawa [38]. The nature of the representation, however, masks some important differences. If the fluid properties are represented in terms of their natural dimensionless variables (Figure 1(b)), it is evident that the LJ system and Model 3, both with corresponding $\alpha = 0.889$, exhibit a very different phase behaviour to that of Models 1 and 2 (of $\alpha = 0.521$), which have a lower critical temperature in these units, and therefore, cannot be said to be conformal with Model 3 or the

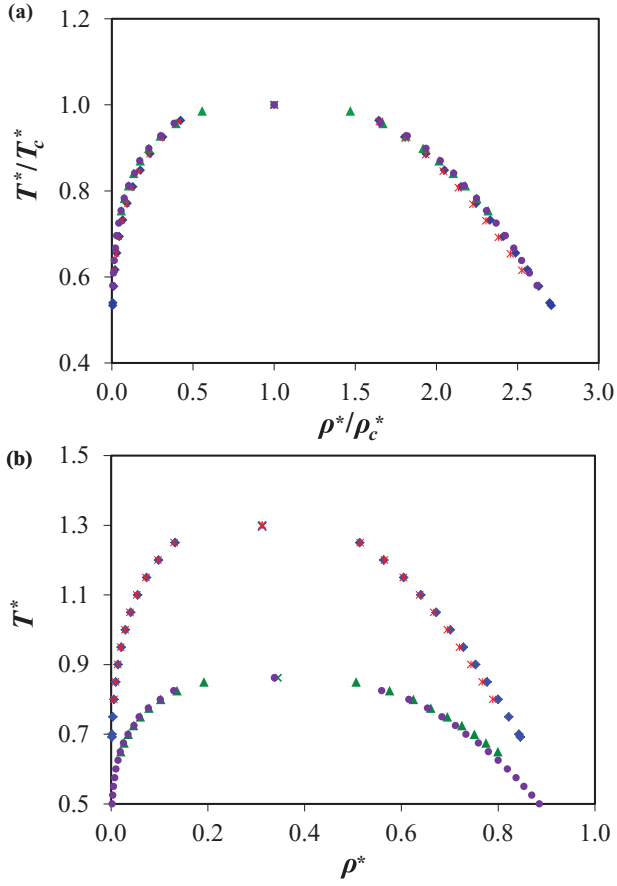

Figure 1. Temperature-density fluid-phase coexistence data obtained by molecular dynamics simulations for Mie potentials: (23.00, 6.66), Model 1, with corresponding $\alpha = 0.521$ (green triangles); (14.65,8.00), Model 2, with the same corresponding $\alpha = 0.521$ (purple circles); Lennard-Jones (12.00,6.00) potential, with corresponding $\alpha = 0.890$ (blue diamonds); and (9.16, 7.00), Model 3, with corresponding $\alpha = 0.890$ (red asterisks). (a) The temperature and density are reduced with respect to the corresponding critical temperature and density; (b) standard dimensionless units $T^* = k_B T/\varepsilon$ and $\rho^* = \rho\sigma^3$ are used. The estimated critical points are indicated with crosses of each respective colour.

Table 1. Vapour-liquid critical properties of Mie intermolecular potential models of repulsive exponent λ_r and attractive exponent λ_a. Models of the same value of α (cf. Equation (13)) present close-to-conformal critical properties. $T_c^* = kT_c/\varepsilon$ is the critical temperature, $\rho_c^* = \rho_c\sigma^3$ the critical density and $P_c^* = P\sigma^3/\varepsilon$ the critical pressure.

Model	λ_r	λ_a	α	T_c^*	ρ_c^*	P_c^*
1	23.00	6.66	0.521	0.864	0.346	0.087
2	14.65	8.00	0.521	0.862	0.338	0.080
LJ	12.00	6.00	0.890	1.312	0.312	0.119
3	9.16	7.00	0.890	1.306	0.312	0.118

LJ model. It is clear, however, that each of the pairs with the same value of the parameter α displays conformal behaviour in the $T^* - \rho^*$ space, as suggested by Equation (12).

The vapour pressures of the four Mie model potentials were also obtained and are shown in Figure 2. In Figure 2(a), the properties are scaled with respect to the corresponding critical temperature and pressure. It is interesting to note that the vapour pressures of the four models, even when reduced with the respective critical properties, do not map onto a unique curve. Instead, two different curves result: higher vapour pressures correspond to the two models with $\alpha = 0.889$ (the LJ system and Model 3); and lower vapour pressures for Models 1 and 2 characterised by a lower value of $\alpha = 0.521$. The four curves are seen to converge at the critical point given the choice of scaling in this representation. In Figure 2(b), the vapour pressures of the four systems are presented in P^* and T^* units and the conformal behaviour of the LJ model and Model 3 on the one hand, and that of Models 1 and 2 on the other, is clearly appreciated. This result rationalises the findings of Galliéro *et al*. [43] who suggested that the vapour pressures of the family of Mie fluids would not follow the CS principle for any arbitrary pairing of exponents; this is consistent with our result in this work, where we demonstrate that only pairs of (λ_r, λ_a) corresponding to the same α follow a CS behaviour.

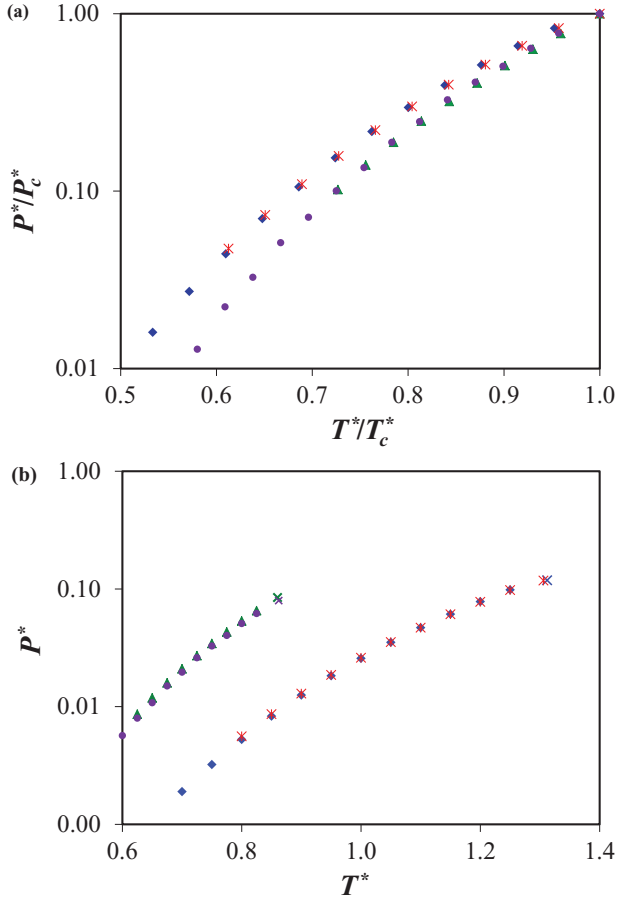

Figure 2. Vapour-pressure data obtained by molecular dynamics simulations for Mie potentials: (23.00, 6.66), Model 1, with corresponding $\alpha = 0.521$ (green triangles); (14.65,8.00), Model 2, with the same corresponding $\alpha = 0.521$ (purple circles); Lennard-Jones (12.00,6.00) potential, with corresponding $\alpha = 0.890$ (blue diamonds); and (9.16, 7.00), Model 3, with corresponding $\alpha = 0.890$ (red asterisks). (a) The pressure and temperature are reduced with respect to the corresponding critical states; (b) standard dimensionless units $P^* = P\sigma^3/\varepsilon$ and $T^* = k_B T/\varepsilon$ are used.

Having confirmed the usefulness of the parameter α to characterise the family of Mie pair potentials, we continue to study now the global (solid, liquid, vapour) phase behaviour of the family for a range of values of this parameter. In Figure 3, the vapour–liquid and solid–fluid phase boundaries are presented, and from these the triple–point temperature, critical–point temperature and the range of temperatures over which the fluid envelope is stable (the 'fluid range') can be seen. In the figure, the phase boundaries of Models 1 and 2, which are conformal as shown in the previous figures in terms of their fluid phase behaviour, are compared to those of the LJ model. In considering the solid phase now it can be seen, that the unique phase behaviour seen in Figure 1(a) does not follow for the solid boundaries even in the representation in terms of the critical conditions. The triple–point temperatures T_t^* of Models 1 and 2 are very close, and therefore, the fluid range T_c^*/T_t^* of the two systems is also very similar; the small differences are likely to be caused by the approximations we have made in the determination of the α parameter. In contrast, the LJ model exhibits a distinctly lower triple temperature and larger fluid range. In Figure 3(b), a similar result is observed when the properties are expressed in units of ε and σ: a much larger fluid envelope is evident for the LJ model by comparison to those of Models 1 and 2. These phase diagrams highlight the non-conformal nature of the solid phase, as originally suggested by Guggenheim [47], but also confirm the validity of our proposed parameter α in rationalising the phase behaviour of the Mie family of potentials, even including the solid–phase behaviour. The

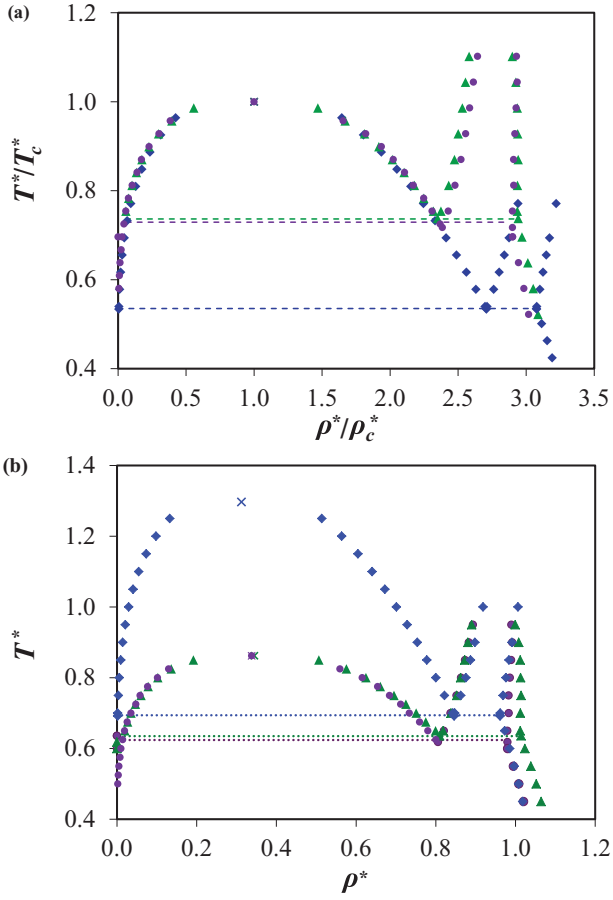

Figure 3. Temperature-density fluid-phase and solid–phase coexistence data obtained by molecular dynamics simulations of two conformal Mie potentials with corresponding $\alpha = 0.521$: (23.00, 6.66), Model 1, (green triangles) and (14.65,8.00), Model 2, (purple circles). Coexistence data for the Lennard-Jones (12.00,6.00) potential, with corresponding $\alpha = 0.890$ (blue diamonds) are shown for comparison. (a) The temperature and density are reduced with respect to the corresponding critical states; (b) standard dimensionless units $T^* = k_B T/\varepsilon$ and $\rho^* = \rho\sigma^3$ are used. The estimated critical points are indicated with crosses of each respective colour.

expression for α presented here is defined strictly from the integration of the average cohesive energy of the potential, with the integration carried out from a value of σ (for which the potential is zero) spanning into the attractive well of the potential to infinite distance under a mean-field approximation. The particles in the solid phase explore the repulsive ($r < \sigma$) region of the potential, and as a result of this, details of the repulsive part of the potential are especially important in the calculation of properties of the solid phase. In our derivation of Section 2, the reference repulsive system was approximated to a hard-sphere system, dependent only on the value of σ (and density) but not on the value of λ_r; the impact of this approximation, together with the mean-field assumption, can be seen here in the small differences

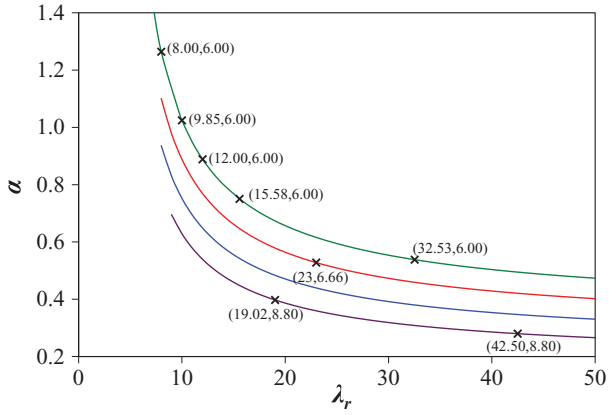

Figure 4. Variation of α as a function of repulsive exponent λ_r of the Mie potential. The purple curve corresponds to (λ_r, 8.80) potentials, the blue curve to (λ_r, 7.50) potentials, the red curve to (λ_r, 6.66) potentials and the green curve to (λ_r, 6.00) potentials. The black crosses indicate the particular potentials chosen in this work for the calculation of their phase boundaries via computer simulation.

observed for the solid boundary properties of Models 1 and 2.

4.2. *Phase behaviour trends of Mie family of pair potentials*

At this point, we select a number of Mie pair potentials of varying range of attraction and which are characterised by unique values of α, and calculate their phase coexistence properties using MD simulations. The systems considered span distinct ranges of the pair potentials from a soft, slow-decaying, attractive tail to a very short-ranged attraction. The parameter space considered is presented in Figure 4 with the systems selected highlighted. The softest potential studied is a Mie (8.00,6.00) model (corresponding to $\alpha = 1.264$) and the most repulsive potential considered is a Mie (42.00,8.80) (corresponding to $\alpha = 0.280$). In particular,

Table 2. Selected Mie pair potentials with exponents λ_r and λ_a and their corresponding α (cf. Equation (13)) value. The critical-point and triple–point temperatures obtained from the analysis of molecular dynamics simulation are presented as well as their ratio T_c^*/T_t^* which provides an indication of the stability range of the vapour-liquid phase envelope.

λ_r	λ_a	α	T_c^*	T_t^*	$\frac{T_c^*}{T_t^*}$
8.00	6.00	1.264	1.743	0.706	2.469
9.85	6.00	1.038	1.456	0.680	2.141
12.00	6.00	0.890	1.312	0.694	1.890
15.58	6.00	0.750	1.113	0.675	1.649
32.53	6.00	0.538	0.869	0.635	1.369
23.00	6.66	0.521	0.864	0.636	1.358
19.02	8.80	0.398	0.735	0.600	1.225
42.50	8.80	0.280	0.585	0.572	1.023

Table 3. Coexistence densities of the gas ρ_g^*, liquid ρ_l^* and solid ρ_s^* phases calculated via computer simulation for the Mie (8.00,6.00) potential at temperatures T^*. The type of phase equilibrium is indicated in the last column along with the estimated (*) triple and critical points. The error is given in square parentheses (e.g., 1.028[9] = 1.028 ± 0.009).

T^*	ρ_g^*	ρ_l^*	ρ_s^*	Phases
0.450	∼0		1.028[9]	SVE
0.500	∼0		1.020[1]	SVE
0.550	∼0		1.010[6]	SVE
0.600	∼0		1.000[7]	SVE
0.650	∼0		0.990[3]	SVE
0.706	0.00016	0.892	0.978	Triple point*
0.800	0.00074[3]	0.862[1]		VLE
0.807		0.924[1]	0.987[9]	SFE
0.850	0.0012[7]	0.846[4]		VLE
0.900	0.0021[2]	0.830[3]		VLE
0.950	0.0042[6]	0.815[1]		VLE
1.050	0.007[1]	0.782[6]		VLE
1.100	0.0107[9]	0.766[2]		VLE
1.150	0.014[1]	0.748[6]		VLE
1.200	0.017[7]	0.730[4]		VLE
1.250	0.022[2]	0.711[9]		VLE
1.300	0.027[9]	0.692[7]		VLE
1.350	0.037[1]	0.671[9]		VLE
1.400	0.046[5]	0.652[2]		VLE
1.500	0.068[9]	0.601[6]		VLE
1.600	0.115[9]	0.546[7]		VLE
1.743	0.296	0.296		Critical point*

Table 4. Coexistence densities of the gas ρ_g^*, liquid ρ_l^* and solid ρ_s^* phases calculated via computer simulation for the Mie (9.85,6.00) potential at temperatures T^*. Metastable points are highlighted with parentheses and the type of equilibrium is indicated in the last column along with the estimated (*) triple and critical points. The error is given in square parentheses (e.g., 1.009[1] = 1.009 ± 0.001).

T^*	ρ_g^*	ρ_l^*	ρ_s^*	Phases
0.450	∼0		1.009[1]	SVE
0.500	∼0		0.999[1]	SVE
0.550	∼0		0.988[5]	SVE
0.600	(0.00009[1])	(0.895)		VLE
0.600	∼0		0.977[1]	SVE
0.650	(0.00044[9])	(0.873[5])		VLE
0.680	∼0	0.869	0.967	Triple point*
0.700		0.870[3]	0.969[6]	SFE
0.700	0.0011[1]	0.856[8]		VLE
0.800	0.0028[1]	0.820[6]		VLE
0.800		0.897[1]	0.983[2]	SFE
0.850		0.912[1]	0.994[1]	SFE
0.900	0.0080[5]	0.780[9]		VLE
0.900		0.923[9]	0.998[6]	SFE
1.000	0.0154[3]	0.739[1]		VLE
1.000		0.946[8]	1.016[3]	SFE
1.100	0.0297[7]	0.692[9]		VLE
1.200	0.050[9]	0.641[7]		VLE
1.300	0.0844[8]	0.578[8]		VLE
1.456	0.293	0.293		Critical point*

seven systems are presented, and the specific values of the exponents (λ_r, λ_a), the critical–point temperatures, triple–point temperatures and fluid ranges are listed in Table 2 (the LJ potential is included for comparison). Using the simulation methodology outlined earlier, the solid–, liquid– and vapour-phase boundaries are calculated carrying out MD simulations; the results are presented in Tables 3–7 for a number of selected systems.

In Figure 5, the vapour–liquid, solid–liquid and solid–vapour phase boundaries for each of the potentials are presented in temperature–density phase diagrams. A representation in T^*/T_c^* units results in an almost unique vapour-liquid equilibrium (VLE) envelope of all potentials (with small differences noted for the gas boundary). This type of representation led Okumura and Yonezawa [38] and subsequently others to suggest that the family of Mie potentials was conformal for any arbitrary value of exponents. When the solid–liquid boundary is also inspected, however, marked differences in the phase behaviour of the systems can be seen, as we noted already in Figure 3. The range of temperatures between the triple point and critical point (the fluid range, T_c^*/T_t^*) varies significantly for the different exponent pairs considered. A trend may be appreciated in the figure suggesting that smaller values of the parameter α, which corresponds to a reduced attractive integrated energy of the potential, leads to a smaller range of temperatures over which the fluid phase is stable. The trend leading to

Table 5. Coexistence densities of the gas ρ_g^*, liquid ρ_l^* and solid ρ_s^* phases calculated via computer simulation for the Mie (15.58,6.00) potential at temperatures T^*. Metastable points are highlighted with parentheses and the type of equilibrium is indicated in the last column along with the estimated (*) triple and critical points. The error is given in square parentheses (e.g., 1.022[2] = 1.022 ± 0.002).

T^*	ρ_g^*	ρ_l^*	ρ_s^*	Phases
0.450	∼0		1.022[2]	SVE
0.500	∼0		1.011[2]	SVE
0.550	∼0		0.996[9]	SVE
0.600	∼0		0.985[7]	SVE
0.650	∼0		0.979[2]	SVE
0.650	(0.00030[7])	(0.845[2])		VLE
0.675	∼0	0.830	0.978	Triple point*
0.700	0.0062[2]	0.817[4]		VLE
0.700		0.838[4]	0.979[1]	SFE
0.750		0.851[6]	0.980[1]	SFE
0.800		0.865[1]	0.982[6]	SFE
0.800	0.0014[7]	0.759[7]		VLE
0.850		0.874[7]	0.984[9]	SFE
0.900		0.886[1]	0.987[3]	SFE
0.900	0.037[5]	0.693[6]		VLE
1.000	0.084[6]	0.609[9]		VLE
1.000		0.903[2]	0.996[2]	SFE
1.050	0.148[5]	0.559[2]		VLE
1.100		0.920[3]	0.998[2]	SFE
1.113	0.324	0.324		Critical point*

Table 6. Coexistence densities of the gas ρ_g^*, liquid ρ_l^* and solid ρ_s^* phases calculated via computer simulation for the Mie (19.02,8.80) potential at temperatures T^*. Metastable points are highlighted with parentheses and the type of equilibrium is indicated in the last column along with the estimated (*) triple and critical points. The error is given in square parentheses (e.g., 1.070[9] = 1.070 ± 0.009).

T^*	ρ_g^*	ρ_l^*	ρ_s^*	Phases
0.350	∼0		1.070[9]	SVE
0.400	∼0		1.060[7]	SVE
0.450	∼0		1.049[8]	SVE
0.500	∼0		1.037[2]	SVE
0.522	(0.0114[8])	(0.864[4])		VLE
0.545	(0.0158[4])	(0.842[1])		VLE
0.550	∼0		1.018[7]	SVE
0.568	(0.0222[3])	(0.819[5])		VLE
0.600	0.030	0.779	1.008	Triple point*
0.613	0.040[6]	0.764[1]		VLE
0.635	0.055[7]	0.736[7]		VLE
0.650		0.803[2]	1.004[4]	SFE
0.658	0.077[3]	0.694[4]		VLE
0.681	0.102[6]	0.646[7]		VLE
0.700		0.827[1]	1.001[1]	SFE
0.704	0.131[9]	0.579[4]		VLE
0.735	0.359	0.359		Critical point*
0.800		0.856[6]	1.005[7]	SFE
0.900		0.875[9]	1.010[2]	SFE
1.000		0.886[6]	1.017[1]	SFE

Table 7. Coexistence densities of the gas ρ_g^*, liquid ρ_l^* and solid ρ_s^* phases calculated via computer simulation for the Mie (42.50,8.80) potential at temperatures T^*. Metastable points are highlighted with parentheses and the type of equilibrium is indicated in the last column along with the estimated (*) triple and critical points. The error is given in square parentheses (e.g., 0.994[8] = 0.994 ± 0.008).

T^*	ρ_g^*	ρ_l^*	ρ_s^*	Phases
0.450	∼0		0.944[8]	SVE
0.500	∼0		0.931[6]	SVE
0.500	(0.043[2])	(0.830[1])		VLE
0.510	(0.052)	(0.821)		VLE
0.520	(0.062)	(0.791)		VLE
0.530	(0.076)	(0.774)		VLE
0.540	(0.092)	(0.741)		VLE
0.545	(0.0158)	(0.842)		VLE
0.550	(0.113)	(0.708)		VLE
0.550	∼0		0.921[5]	SVE
0.560	(0.140)	(0.675)		VLE
0.563		(0.589[3])	(0.920[1])	SFE
0.572	0.190	0.602	0.919	Triple point*
0.585	0.393	0.393		Critical point*
0.600		0.649[7]	0.917[7]	SFE
0.625		0.666[6]	0.915[4]	SFE
0.650		0.687[7]	0.912[5]	SFE
0.700		0.703[3]	0.906[6]	SFE
0.750		0.716[5]	0.908[4]	SFE
0.850		0.732[1]	0.909[4]	SFE
0.950		0.745[9]	0.906[1]	SFE

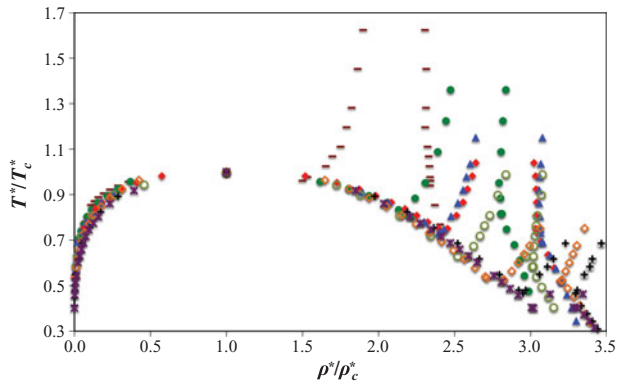

Figure 5. Temperature-density coexistence data for the vapour-liquid, solid-liquid and solid-gas phase boundaries obtained by molecular dynamics simulations for Mie (λ_r, λ_a) potentials: (8.00,6.00) (asterisks); (9.85,6.00) (crosses); (12.00,6.00) (open diamonds); (15.58,6.00) (open circles); (32.53,6.00) (filled triangles); (23.00,6.66) (filled diamonds); (19.02,8.80) (filled circles) and (42.50,8.80) (horizontal dashes). The temperature and density are reduced with respect to the corresponding critical states.

the disappearance of the VLE envelope is seen more clearly in Figure 6, where the phase diagrams of six of the systems are presented in the T^*–ρ^* plane; a similar trend is presented for the Mie ($\lambda_r = 2\lambda_a$,λ_r) family in [34]. In the case of the softest potential considered ($\alpha = 1.264$), with exponents (8.00,6.00) and the larger attractive tail, a large fluid range of $T_c^*/T_t^* = 2.469$ is found. Conversely, in the system with a Mie pair potential of exponents (42.50,8.80) and corresponding $\alpha = 0.280$, the triple and critical temperatures almost coincide ($T_c^*/T_t^* = 1.023$), and a vanishing fluid envelope is observed. We note that an inter-relation exists between the critical-point and triple–point temperatures, and the gradual decrease in α which results in the shrinking of the fluid range until it becomes entirely metastable with respect to the solid phase for a potential of corresponding $\alpha = 0.269$ (44.20,9.00).

Indeed, an interesting trend emerges between the triple and critical temperatures and α when represented against each other (Figure 7(a)). A linear relation of positive slope is seen in the values of the calculated critical temperature with respect to α. The critical and triple temperatures of the systems considered by Okumura and Yonesawa [38], Orea *et al*. [39] and Ahmed and Sadus [36] are also included for comparison. Using the data presented in Table 2, we find that the relation for the critical temperature corresponds to

$$T_c^* = 1.173\alpha + 0.254. \quad (17)$$

The triple-point temperature also increases with increasing α, although with a much smaller gradient, following the relation

$$T_t^* = 0.131\alpha + 0.557. \quad (18)$$

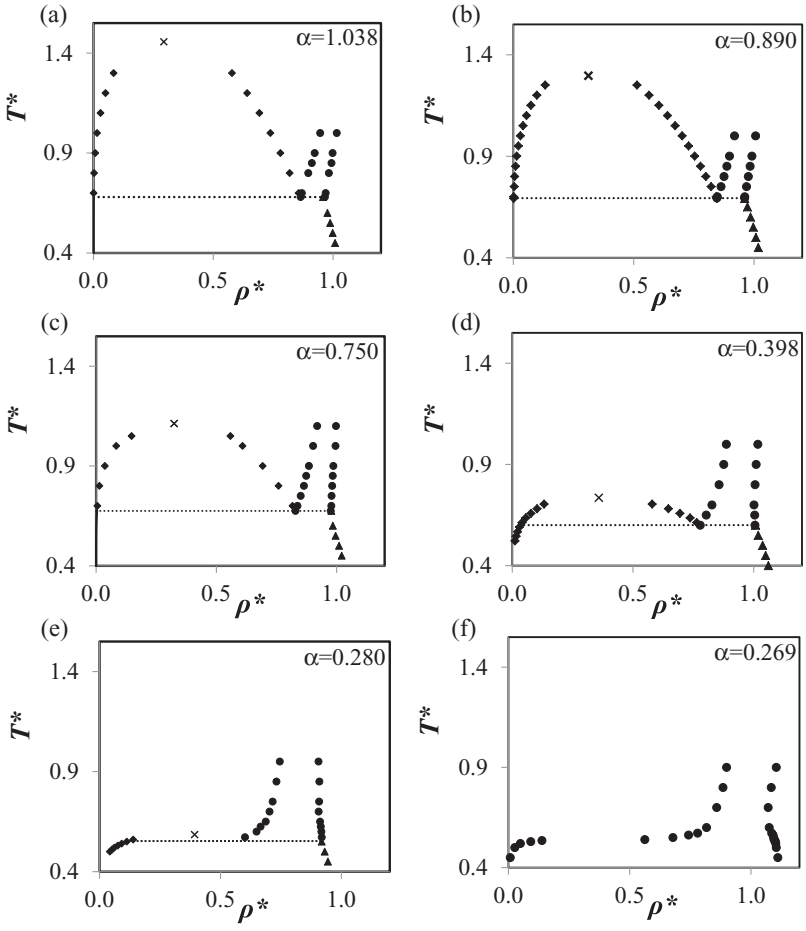

Figure 6. T^*–ρ^* coexistence data for the vapour-liquid, solid-liquid and solid-gas phase boundaries obtained by molecular dynamics simulations for Mie (λ_r, λ_a) potentials in order of decreasing α (cf. Table 2): (a) (9.85,6.00), (b) (12.00,6.00), (c) (15.58,6.00), (d) (19.02,8.80), (e) (42.50,8.80) and (f) (44.20,9.00).

The intersection of these two lines provides the value of α (and hence determines the set of pairs of Mie exponents) below which the VLE region would be found to be metastable. The range of temperatures between the two lines provides a representation of the decrease in size of the stable VLE region with a decreasing value of α. Clearly, the critical–point temperature (T_c^*) appears to be more dramatically influenced by a change in α which may be explained by the fact that α quantifies the size of the attractive well of the potential. This dependence of T_c^* has previously been reported by several authors [35,38,41]. Given the linear trends observed for both the critical–point temperature and the triple-point temperature, a direct linear relation in terms of the conformal parameter α can be proposed for the extent of the fluid range, as defined by T_c^*/T_t^*; this is represented in Figure 7(b). This is in our view a very useful result. In effect, it suggests that for any value of α, and by association any Mie pair potential chosen, the corresponding fluid range can be directly determined with a linear relationship which can be expressed by the following relation:

$$\frac{T_c^*}{T_t^*} = 1.462\alpha + 0.603, \tag{19}$$

and is worth noting that the ratio of temperatures can be equally written as a ratio of experimental temperatures, since the parameter ε cancels in the expression above. Using this equation, the Mie potential for which the fluid envelope becomes metastable with respect to the solid can be easily determined, since it corresponds to the case $T_c^*/T_t^*=1$ ($\alpha = 0.269$). In Figure 6(f), the phase diagram of a Mie potential with $\alpha = 0.269$ and exponents (44.20,9.00) is presented. The exponent pair chosen (44.20,9.00) is arbitrary and any pair corresponding to the same value of α would give similar results. As can be seen in the figure, no stable liquid region is observed, as predicted. This result may be compared to the potentials determined by Hasegawa [32] and Hasegawa and Ohno [33] who also investigated the values of exponents in the Mie pair potential that would lead to a metastable fluid region. Hasegawa and Ohno[33] determined such a potential using a density functional theory of freezing and found the potential to be (24.00,12.00), which corresponds to $\alpha = 0.254$. When a variational perturbation theory is used instead of the density functional theory, Hasegawa [32] determined the potential for the metastability of the VLE region to be (28.00,14.00) ($\alpha = 0.204$). These points have

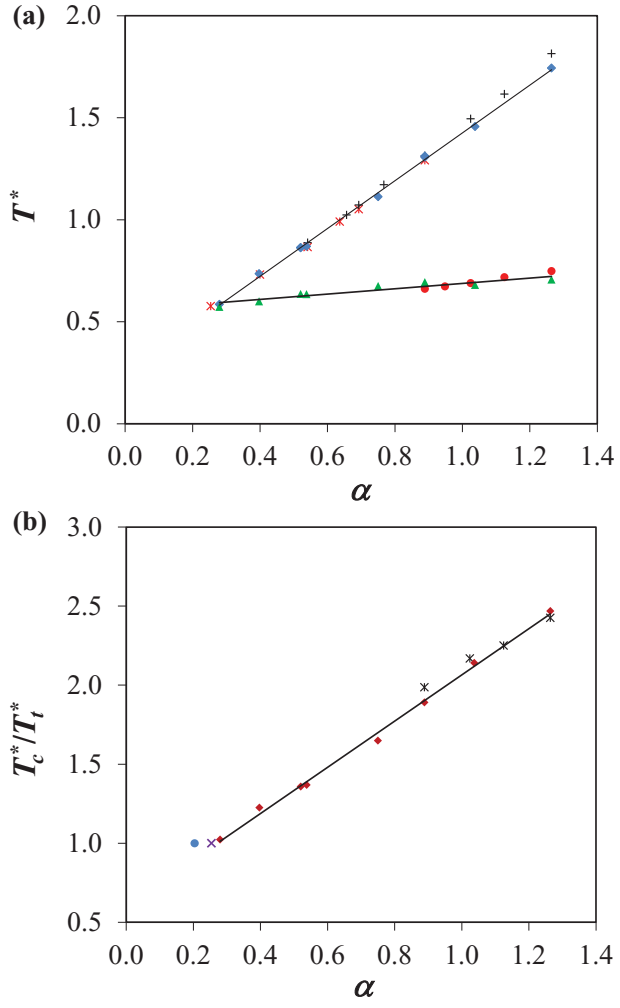

Figure 7. (a) Critical temperature T_c^* (diamonds) and triple temperature T_t^* (triangles) as a function of α for the systems considered (cf. Table 2). For comparison, the critical temperature data of Orea *et al*. [39] are shown as red asterisks and those of Okumura and Yonesawa [38] as black crosses. The triple–point temperatures of Ahmed and Sadus [36] are shown as solid red circles. The solid lines correspond to the linear relations in Equations (17) and (18). (b) Fluid range T_c^*/T_t^* as a function of α (diamonds) for the systems selected in this work. The temperature ratios indicated with the asterisks are obtained using the critical temperatures of Okumura and Yosenawa and the triple temperatures calculated by Ahmed and Sadus. The solid line corresponds to the linear relation in Equation (19). The value of α at which the VLE region becomes metastable as determined by Hasegawa [32] is indicated with a filled (blue) circle and that of Hasegawa and Ohno [33] with a purple asterisk.

been included in Figure 7(b) for comparison to the potential determined in this work. Both are in effect in agreement with our result, as they correspond to lower values of α to the one we find with our proposed conformal parameter. The agreement is reassuring, considering that the studies used the ($\lambda_r = 2\lambda_a$, λ_a) classification with only potentials with exponents of integer values being considered.

4.3. *Application to coarse-grained potentials for real systems*

The use of the Mie potential to calculate the properties of real systems requires the determination of four parameters, σ, ε, λ_r and λ_a, which, on first inspection, appear independent of each other. It was shown in Section 2, however, that λ_r and λ_a can be related by Equation (13) to provide an essentially identical free energy (within approximations). In addition, in modelling real systems, if one is willing to specify the fluid range T_c/T_t, by means of Equation (19), α is determined and limits the choice of exponent pairs that may be considered in order to obtain a range of stability for the fluid envelope which is consistent with that of the real system. If one of the exponents is specified, the other one is then determined from these relations.

An example is provided in Figure 8 for three molecules (carbon dioxide CO_2, water H_2O and buckminsterfullerene C_{60}) that have been modelled using coarse-grained spherical potentials [17,69] and for the LJ model for comparison. The ratios of the critical-point and triple–point temperatures with their corresponding values of the parameter α are indicated. The fluid range of carbon dioxide ($T_c^{\rm exp} = 304.25$ K, $T_t^{\rm exp}$=216.55 K, $T_c/T_t = 1.405$) corresponds to $\alpha = 0.545$. In the figure, curves corresponding to potentials with values of the attractive Mie exponent $\lambda_a = 6$, 7, 8 and 10 for varying λ_r (varying α) are indicated. It can be seen that the corresponding fluid range ratio, or value of α, of CO_2 intersects the three curves that correspond to (λ_r, 6), (λ_r, 7) and (λ_r, 8). Each of these pairs would lead to a coarse–grained model potential for CO_2 with a fluid range in agreement to that of the experimental system. This suggests that the thermodynamic properties of CO_2 can be accurately described using a spherical (31.00,6.00), or a (18.00,7.00) or

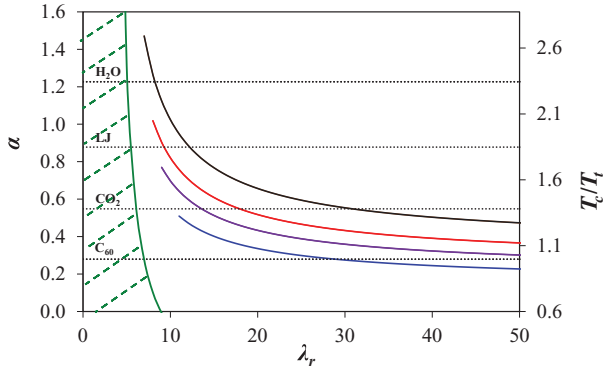

Figure 8. Variation of α and corresponding fluid range (T_c^*/T_t^*) with Mie fluids of fixed attractive exponents; (λ_r, 6.00) is represented by a solid black curve, (λ_r, 7.00) with a red curve, (λ_r, 8.00) with a purple curve and (λ_r, 10.00) a blue curve. The dashed lines indicate the experimental fluid range of H_2O and CO_2 , that of the reference LJ potential, and that of the coarse–grained model for C_{60}. The shaded region represents exponent combinations where $\lambda_a > \lambda_r$ in which the potentials are unrealistic.

(13.50,8.00) Mie pair potential with roughly equivalent accuracy. Although the parameters may be obtained from least square fitting of experimental data such as vapour pressure and liquid densities [17], the parameter space is large and the solution is not unique. Moreover, as the properties of the solid are not usually considered in such parameter fits, the resulting models often do not exhibit a fluid range in agreement with that of the experimental system. The model in [17] is characterised by the pair of exponents (23.00,6.66), which leads to a corresponding $\alpha = 0.521$, slightly lower than that of the experimental system meaning that freezing will occur at higher temperatures than expected if the value of the parameter ε is determined seeking agreement with the critical temperature. Being able to propose exponent pairs *a priori* which are self–consistent will enable more robust parameters to be obtained from this fitting procedure. Once the exponent set is fixed, the critical temperature and a liquid density [70] are sufficient to specify the values of ε and σ, respectively. For example, choosing the pair (18.00,7.00), values of $\varepsilon/k_B = 376\ K$ and $\sigma = 3.82$ Å provide a suitable although, again, not unique set of parameters representing a spherical coarse–grained model for CO_2 with a fluid range in closer agreement to that of experiment.

In the case of water, the phase behaviour and thermodynamic properties are highly anomalous as a result of the strong intermolecular interactions brought by the presence of the network of hydrogen bonds that forms in the liquid phase. Attempts to develop a coarse-grained model for this molecule based on a spherical Mie potential to treat its thermodynamic properties, including its vapour pressure, lead to a potential with a very large repulsive exponent when a traditional fit to saturated properties is carried out [69]. The resulting model is seen to present freezing at temperatures well above the triple point of water, which, in effect, renders it unsuitable for fluid-phase calculations. This is an example where the traditional top-down coarse–graining technique can struggle to give a satisfactory result. The premature freeze may, however, be preempted by considering the alternative approach proposed here, in which a value of the constant α is first calculated using the experimental critical and triple temperatures together with Equation (19), which leads to $\alpha = 1.203$. If one is to choose an attractive exponent $\lambda_a = 6.00$, the corresponding repulsive exponent through Equation (13) is $\lambda_r = 8.40$ [70]. A single-site coarse-grained model of water is also presented in a separate work in this Issue [69], and it is shown to provide an accurate model for water, especially when a temperature dependence is incorporated in ε and σ.

The buckminsterfullerene C_{60} molecule provides another interesting example. The functional form proposed by Girifalco [27] provides a good representation of its thermodynamic properties based on a spherical potential of depth $\varepsilon/k_B = 3218$ K and $\sigma = 9.59$ Å, which is steeper and shorter ranged that the LJ potential. Hagen *et al*. [28] showed that this potential leads to a phase diagram where the vapour– liquid envelope is metastable with respect to a solid– fluid transition. A similar result was also found by Cheng *et al*. [71], although these authors report a small range of temperatures over which stable vapour– liquid transitions are obtained. The shape of the potential first reported by Girifalco can also be adjusted to a Mie pair potential; we find that a coarse–grained Mie potential characterised by $\varepsilon/k_B = 3213.5$ K, $\sigma = 9.05$ Å, $\lambda_r = 42.50$ and $\lambda_a = 8.80$ provides a good fit. In this work, we have used these potential parameters to determine the phase diagram of C_{60} via molecular simulation. The result was presented in Figure 6(e); it is consistent with the previous calculations of Hagen *et al*. and Cheng *et al*. in that we find a very small stable VLE region with a corresponding ($T_c^*/T_t^* = 1.04$). Examining again Figure 8 it is also apparent that there are other combinations of exponents of the Mie family of potentials that may be used to model the phase behaviour of C_{60}.

5. Conclusion

The solid-, liquid- and gas-phase boundaries of the Mie family of intermolecular potentials have been studied by MD simulations with the aim of obtaining a unified view of this family of systems. By analysis of the Helmholtz free energy using a Barker–Henderson perturbation expansion up to first order and using a mean-field approximation, a parameter α is proposed which characterises the free energy of a given Mie system. Mie potentials with the same value of this parameter α are shown to display close-to-conformal phase behaviour. Slight deviations between the phase boundaries are noted and can be accounted for within the approximations made in the derivation of α. This result contradicts the reports of Orea *et al*. [39] and Okumura and Yonezawa [38] who suggest that the Mie family will follow a two–parameter conformal model for any pair of exponents. It is, however, in agreement with the works of Galliéro *et al*. [20], Bulavin and Kulinskii [41] and Kulinskii [42] who suggest that three parameters are needed to characterise uniquely these systems. The use of the parameter α proposed here provides a rational framework for the characterisation of the phase behaviour of this family of potentials.

By characterising the potential through the α parameter, a host of Mie potentials of varying range of attraction has been studied. The choice of α has a strong influence on the critical point, which is in accordance with the works of Lekkerkerker and co-workers [34,35], Okumura and Yonezawa [38] and Bulavin and Kulinskii [41]. The parameter is noted to have a less significant, although also noticeable, influence on the triple–point temperature. There is a linear relationship between α and the range of temperatures in which a stable fluid envelope is observed (referred to as the fluid range). We find that smaller values of α, which correspond to an increase in the repulsive nature of

the interaction, result in a decrease in the size of the stable fluid range. This result is in agreement with the findings of several other authors [32–34,41,42]. A relationship is derived that can be used to propose the limit at which the fluid envelope region becomes metastable with respect to the solid–fluid phase boundary. The resulting potential in this limit is found to be in good agreement with simulation data and with the theoretical predictions of Hasegawa [32] and Hasegawa and Ohno [33].

Furthermore, the relationship between α and the stable fluid range is especially relevant in the development of coarse-grained models for real systems when a spherical Mie potential is used. We propose a method based on knowledge of the experimental triple and critical temperatures, which is used to determine the unique value of the parameter α that leads to a fluid range of the model system in agreement to that of the experimental system. This limits the Mie exponents that can be used to treat the real system and reduces the parameter space which is typically explored in order to find reliable molecular models to mimic the behaviour of a given real system, including the appearance of the solid phase.

Acknowledgements

The authors would also like to acknowledge the help of S. Dufal and S. Rahman in re-checking some of the calculations. The simulations described herein were performed using the facilities of the Imperial College High-Performance Computing Service.

Disclosure statement

No potential conflict of interest was reported by the authors.

Funding

N.S. Ramrattan would like to thank the Engineering and Physical Sciences Research Council (EPSRC) of the UK for the award of a Doctoral Training Grant. The authors would also like to acknowledge financial support for the Molecular Systems Engineering Group from the EPSRC [grant number EP/E016340], [grant number EP/J014958], [grant number EP/I018212].

References

[1] J.E. Lennard-Jones, Proc. Phys. Soc. **43**, 461 (1931).
[2] W. Sutherland, Philos. Mag. **36**, 507 (1893).
[3] H.W. Graben and R.D. Present, Rev. Mod. Phys. **36**, 1025 (1964).
[4] J.S. Rowlinson, Phys. A **156**, 15 (1989).
[5] P.M. Morse, Phys. Rev. **34**, 57 (1929).
[6] R.A. Buckingham, Proc. R. Soc. Lond A **168**, 264 (1938).
[7] J.E. Jones, Proc. R. Soc. Lond. **106**, 463 (1924).
[8] F. London, Trans. Faraday Soc. **33**, 8 (1937).
[9] F. London, J. Chem. Phys. **46**, 305 (1942).
[10] G. Mie, Ann. Phys. **316**, 1521 (1903).
[11] J.C. Shelley, M.Y. Shelley, R.C. Reeder, S. Bandyopadhyay, and M.L. Klein, J. Chem. Phys. **105**, 4464 (2001).
[12] S.O. Nielsen, C.F. Lopez, G. Srinivas, and M.L. Kein, J. Chem. Phys. **119**, 7043 (2003).
[13] M. McCullagh, T. Prytkova, S. Tonzani, N.D. Winter, and G.C. Schatz, J. Chem. Phys. **112**, 10388 (2008).
[14] J.J. Potoff and D.A. Bernard-Brunel, J. Phys. Chem. B **44**, 14725 (2009).
[15] T. Lafitte, A. Apostolakou, C. Avendaño, A. Galindo, C.S. Adjiman, E.A. Müller, and G. Jackson, J. Chem. Phys. **139**, 154504 (2013).
[16] J. Israelachvili and M. Ruths, Langmuir **29**, 9605 (2013).
[17] C. Avendaño, T. Lafitte, A. Galindo, C.S. Adjiman, G. Jackson, and E.A. Müller, J. Phys. Chem. B **115**, 11154 (2011).
[18] T. Lafitte, D. Bessieres, M.M. Piñeiro, and J.L. Daridon, J. Chem. Phys. **124**, 024509 (2006).
[19] P. Paricaud, J. Chem. Phys. **124**, 154505 (2006).
[20] G. Galliéro, T. Lafitte, D. Bessieres, and C. Boned, J. Chem. Phys. **127**, 184506 (2007).
[21] C.G. Aimoli, E.J. Maginn, and C.R.A. Abreu, Fluid Phase Equilib. **368**, 80 (2014).
[22] C.G. Aimoli, E.J. Maginn, and C.R.A. Abreu, J. Chem. Eng. Data **59**, 3041 (2014).
[23] C.G. Aimoli, E.J. Maginn, and C.R.A. Abreu, J. Chem. Phys. **141**, 134101 (2014).
[24] C. Avendaño, T. Lafitte, A. Galindo, C.S. Adjiman, G. Jackson, and E.A. Müller, J. Phys. Chem. B **117**, 2717 (2013).
[25] T. Lafitte, C. Avendaño, V. Papaioannou, A. Galindo, C.S. Adjiman, G. Jackson, and E.A. Müller, Mol. Phys. **110**, 1189 (2012).
[26] E.A. Müller and G. Jackson, Ann. Rev. Chem. Biomol. Eng. **5**, 405 (2014).
[27] L.A. Girifalco, J. Chem. Phys. **96**, 858 (1992).
[28] M.H.J. Hagen, E.J. Meijer, G.C.A.M. Mooij, D. Frenkel, and H.N.W. Lekkerkerker, Nature **365**(5), 425–426 (1993).
[29] A.Z. Panagiotopoulos, Mol. Phys. **61**, 813 (1987).
[30] D.A. Kofke, J. Chem. Phys. **98**, 1 (1993).
[31] M.H.J. Hagen and D. Frenkel, J. Chem. Phys. **101**, 4093 (1994).
[32] M. Hasegawa, J. Chem. Phys. **108**, 208 (1997).
[33] M. Hasegawa and K. Ohno, J. Phys. Condens. Matter **9**, 3361 (1997).
[34] G.A. Vliegenthart, J.F.M. Lodge, and H.N.W. Lekkerkerker, Phys. A **263**, 378 (1999).
[35] G.A. Vliegenthart and H.N.W. Lekkerkerker, J. Chem. Phys. **112**, 5364 (2000).
[36] A. Ahmed and R.J. Sadus, J. Chem. Phys. **131**, 1 (2009).
[37] R.J. Larsen and C.F. Zukoski, J. Chem. Phys. **136**, 054901 (2012).
[38] H. Okumura and F. Yonesawa, J. Chem. Phys. **113**, 9162 (2000).
[39] P. Orea, Y. Reyes-Mercado, and Y. Duda, Phys. Lett. A **372**, 7024 (2008).
[40] A. Gil-Villegas, F. del Río, and A.L. Benavides, Fluid Phase Equilib. **119**, 97 (1996).
[41] L.A. Bulavin and V.L. Kulinskii, J. Chem. Phys. **113**, 134101 (2010).
[42] V. L. Kulinskii, J. Chem. Phys. **134**, 144111 (2011).
[43] G. Galliéro, C. Boned, A. Baylaucq, and F. Montel, Phys. Rev. E **73**, 061201 (2006).
[44] G. Galliéro, M.M. Piñeiro, B. Mendiboure, C. Miqueu, T. Lafitte, and D. Bessieres, J. Chem. Phys. **130**, 104704 (2009).
[45] J.D. van der Waals, Z. Phys. Chem. **13**, 657 (1894).
[46] H. Kamerlingh-Onnes, Comm. Phys. Lab. Univ. Leiden **120b** (1911).
[47] E.A. Guggenheim, J. Chem. Phys. **13**, 253 (1945).
[48] G.J. Su, Ind. Eng. Chem. **38**, 803 (1946).
[49] K.S. Pitzer, J. Chem. Phys. **7**, 583 (1939).

[50] T.M. Reed and K.E. Gubbins, *Applied Statistical Mechanics* (McGraw-Hill Inc., New York, 1973).
[51] T.W. Leland and P.S. Chapplear, Ind. Eng. Chem. **60**, 17 (1968).
[52] H.C. Longuet-Higgins, Proc. R. Soc. Lond. Ser. A **205**, 247 (1951).
[53] W.B. Brown, Philos. Trans. R. Soc. Lond. Ser. A **250**, 175 (1957).
[54] A. Gil-Villegas, A. Galindo, P.J. Whitehead, S.J. Mills, G. Jackson, and A.N. Burgess, J. Chem. Phys. **106**, 4168 (1997).
[55] J.A. Barker and D. Henderson, J. Chem. Phys. **47**, 4714 (1967).
[56] J.A. Barker and D. Henderson, J. Chem. Phys. **47**, 2856 (1967).
[57] N.F. Carnahan and K.E. Starling, J. Chem. Phys. **51**, 635 (1969).
[58] K.R. Hall, J. Chem. Phys. **57**, 2252 (1972).
[59] T. Boublík, J. Chem. Phys. **53**, 471 (1970).
[60] W. Smith and T.R. Forrester, J. Mol. Graph. **14**, 136 (1996).
[61] L.F. Vega, E. de Miguel, L.F. Rull, G. Jackson, and I.A. McLure, J. Chem. Phys. **96**, 2296 (1991).
[62] N. Ramrattan, A. Galindo, and E.A. Müller, 2014 (manuscript in preparation).
[63] U. Agarwal and F.A. Escobedo, Nat. Mater. **10**, 230 (2011).
[64] J.M. Morris and X. Song, J. Chem. Phys. **116**, 1 (2002).
[65] C. Vega, M. Martín-Conde, and A. Patrykiejew, Mol. Phys. **104**, 3583 (2006).
[66] M. Nayhouse, J. Sang-Il Kwon, V.R. Heng, A.M. Amlani, and G. Orkoulas, Int. J. Thermophys. **141**, 134101 (2014).
[67] S. Luo, A. Strachan, and D. Swift, J. Chem. Phys. **120**, 11640 (2004).
[68] M. Parrinello and A. Rahman, Phys. Rev. Lett. **45**, 1196 (1980).
[69] O. Lobanova, C. Avendaño, T. Lafitte, G. Jackson, and E.A. Müller, Mol. Phys. D.O.I. 10.1080/00268976.2015.1004804 (2015).
[70] A. Mejía, C. Herdes, and E.A. Müller, Ind. Eng. Chem. Res. **53**, 4131 (2014).
[71] A. Cheng, M.L. Klein, and C. Caccamo, Phys. Rev. Lett. **71**, 1200 (1993).